

DMRG study of strongly interacting \mathbb{Z}_2 flatbands: a toy model inspired by twisted bilayer graphene

P. Myles Eugenio^{1,2,*} and Ceren B. Dağ³

¹*National High Magnetic Field Laboratory, Tallahassee, Florida, 32304, USA*

²*Department of Physics, Florida State University, Tallahassee, Florida 32306, USA*

³*Department of Physics, University of Michigan, Ann Arbor, Michigan 48109, USA*

Strong interactions between electrons occupying bands of opposite (or like) topological quantum numbers (Chern = ± 1), and with flat dispersion, are studied by using lowest Landau level (LLL) wavefunctions. More precisely, we determine the ground states for two scenarios at half-filling: (i) LLL's with opposite sign of magnetic field, and therefore opposite Chern number; and (ii) LLL's with the same magnetic field. In the first scenario – which we argue to be a toy model inspired by the chirally symmetric continuum model for twisted bilayer graphene – the opposite Chern LLL's are Kramer pairs, and thus there exists time-reversal symmetry (\mathbb{Z}_2). Turning on repulsive interactions drives the system to spontaneously break time-reversal symmetry – a quantum anomalous Hall state described by one particle per LLL orbital, either all positive Chern $|+\dots+\rangle$ or all negative $|-\dots-\rangle$. If instead, interactions are taken between electrons of like-Chern number, the ground state is an $SU(2)$ ferromagnet, with total spin pointing along an arbitrary direction, as with the $\nu = 1$ spin- $\frac{1}{2}$ quantum Hall ferromagnet. The ground states and some of their excitations for both of these scenarios are argued analytically, and further complimented by density matrix renormalization group (DMRG) and exact diagonalization.

I. INTRODUCTION

The unprecedented nature of the phenomena exhibited by twisted bilayer graphene (TBG) devices at various electron densities about charge neutrality (CN), including correlated insulating states [1–3] and superconductivity [4, 5], has opened the door to many experimental [1–7] and theoretical [8–21] studies since their initial discovery by *Y. Cao, et al* [1, 4] in 2018. Unlike band insulators, which occur when the Fermi energy falls in the gap between bands of a periodic crystal, fully occupying the lower band with electrons, these correlated insulating states are a result of (and cannot be described without) interactions, and can occur at any integer filling of a band. These strong repulsive interactions allow the electronic energy to be minimized by separating the particles as far apart as possible, producing a localized state necessary for insulation [22, 23]. Of principle importance to such an interaction dominated paradigm is the presence of flat or nearly flat bands [24], with bandwidths smaller than the interaction energy. In TBG, and similarly other Moire heterostructures (MHS) [25–29], such nearly flat bands are the result of an emergent long-range periodic potential. The $l_M \sim 13\text{nm}$ periodic potential in TBG forms out of the overlap between two stacked single-layer honeycomb lattices, relatively twisted at magic angles [8, 12, 25, 26]. Multiple theoretical estimates place the bandwidth in TBG to be no larger than 10 meV [8–10], smaller than the ~ 23 meV Coulomb energy observed by Scanning Tunneling Microscopy (STM) [6, 7].

While the above prescription for an insulator – minimization of the interaction energy by localizing the elec-

trons – seems straightforward, it is complicated by the topologically non-trivial nature of the nearly flat bands [10, 12, 25]. In two dimensions, a complete orthonormal set of single-particle states, which are exponentially localized in both directions, cannot be constructed from bands carrying non-zero Chern number [10, 12, 19, 25]. Roughly speaking, one can understand this non-trivial topology in analogy with the quantum Hall (QH) [30–37], in which the Landau levels have zero dispersion and Chern number ± 1 , depending on the sign of the magnetic field. As such, there exists a gauge similar to the Landau gauge, which preserves localization in one direction, albeit sacrificing localization in the other, i.e the hybrid Wannier states [38–41].

However, while topological, the total Chern number of the narrow bands in TBG is zero. This can be understood within the continuum model of TBG [8], where the like-valley valence and conduction bands carry opposite Chern number $C = \pm 1$, and are guaranteed to touch by the combination of a 180° rotation and time-reversal ($C_{2z}T$) [8, 9, 12, 13, 15, 17]. Yet unlike a topologically trivial system, it is possible to construct pairs of hybrid Wannier states which carry opposite Chern numbers, and which map into each other under $C_{2z}T$ [18]. If we consider again the QH, this would amount to having both the LLL and its $C_{2z}T$ -partner, the latter being just the same Landau level wavefunction with opposite sign of the magnetic field, and which is designated by the group \mathbb{Z}_2 .

In order to make such an analogy with the QH more precise, let us consider the limit of the chirally symmetric continuum model (CSCM) [15], where the narrow bands within the same valley are everywhere degenerate and *exactly* flat. Special to this limit, opposite Chern bands within the same valley are graphene sublattice polarized [15, 18]. This suggests that a sublattice anisotropy (i.e breaking C_{2z} [2, 3, 16]) would split the intra-valley de-

* eugenio@magnet.fsu.edu

generacy into two separated flat bands of opposite Chern number, each with a degenerate time-reversal partner living in the other valley. Depending on the size of their gap Δ relative to the strength of the interaction, two such scenarios emerge in which \mathbb{Z}_2 LLL's as an analogy is inspired: (1) If the gap due to Δ is larger than the interaction strength, and thus mixing between the conduction and valence bands is suppressed. Despite the broken $C_{2z}T$ symmetry, the time-reversal symmetry guarantees that bands of opposite valleys are Kramer pairs [16]. Or (2), the chiral limit with $\Delta = 0$, where the conduction and valence bands are flat and degenerate everywhere. And thus Kramer pairs exist both between and within a valley.

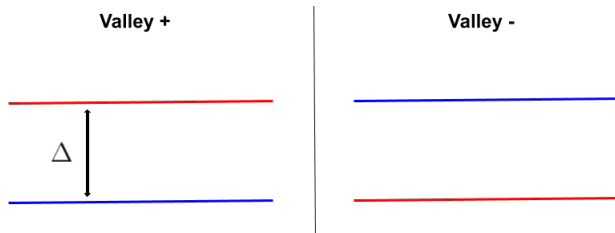


FIG. 1. Two flat Chern bands per valley: red (blue) bands are Chern +1 (-1). The exact order depending on the sign of Δ . Time-reversal symmetry guarantees valley degeneracy even if C_{2z} is broken.

Not counting the spin degree of freedom, the total degeneracy of Scenario (1) and (2) is two and four respectively. The larger degeneracy in the latter brings with it more integer fillings and possible phases; however, for the purposes of this study, we focus on Scenario (2) and assume valley polarization, such that there is only a single intra-valley Kramer pair. In this limit, Scenario (1) and (2) have the same degeneracy structure, both describing an interacting system of fermions occupying opposite-Chern bands. It was previously pointed out by *Bultinck, Chatterjee, and Zaletel* [16] that such a system resembles a bilayer QH problem [36, 37] with one flux quantum per unit cell [16], except with opposite layers (here Chern numbers) experience opposite-sign magnetic fields.

In the original bilayer QH problem, a small anisotropy of the inter-layer repulsive interaction appears as an attraction between electrons and holes in opposite layers, and consequently the system is unstable towards the formation of an inter-layer coherent state [16, 36, 37]. As such, one might be led to believe that strong interactions between \mathbb{Z}_2 LLL's would too lead to a Chern zero state; however, as was previously explored with mean field theory [16], and we show here both analytically and numerically, this is not the case. The ground state is Chern-polarized and stable.

In this paper, we construct the toy model for strongly interacting opposite-Chern flat bands using continuum LLL wavefunctions. We focus our study on $\nu = 1$ electrons per flux quantum, and ask: (i) Is the ground state a

Chern polarized (quantum anomalous Hall) state? And (ii) is such a state stable, unlike the bilayer QH problem? We argue analytically that in the presence of repulsive interactions, the system will choose a Chern insulator, owing to the decomposition of the interaction into a sum of positive semi-definite terms [10, 17], which always favours one flavor of electron per single-particle orbital. Because of the \mathbb{Z}_2 symmetry, there are two such Chern polarized states in the ground state, which we denote: $|++\dots+\rangle$ and $|--\dots-\rangle$.

Additionally, we study the case involving distinct fermions with identical Chern number, but distinguished by an introduced pseudospin $\{\uparrow, \downarrow\}$. In the absence of any interaction anisotropy, this system is identical to the well studied $\nu = 1$ spin- $\frac{1}{2}$ QH ferromagnet [30, 34, 36]. We show the ground state is spin-polarized with one particle per LLL orbital, i.e. $|\uparrow\uparrow\dots\uparrow\rangle$, in addition to a degenerate manifold of states, extensive in the system size, connected by $SU(2)$ rotations. Opposite pseudospins may be taken to represent opposite layers of the bilayer QH problem [36, 37], where both layers experience the *same* sign of the magnetic field. Thus the bilayer QH problem would be unstable against an inter-layer anisotropy, which would break the $SU(2)$ symmetry and split the extensively degenerate manifold in favour of a layer-coherent state. In comparison, the ground state manifold of the \mathbb{Z}_2 QH problem is doubly degenerate, independent of the system size. Therefore, so long as a gap separates its ground state manifold from the higher excited states, the \mathbb{Z}_2 system would be stable.

In order to confirm the existence of a gap, we utilize DMRG [17, 42–49] and exact diagonalization (ED) [17]. This is done by rolling our system into a cylinder, and utilizing the Landau gauge [32] to project our 2D continuum interactions into 1D discrete pseudopotentials [33]. Such a mapping is possible because of the topological non-trivial nature of the LLL's [42–46], and allows us to think of the LLL orbitals as slicing the cylinder into a 1D chain of “sites”, with each site corresponding to the center of a LLL wavefunction (Fig 2). We converge to the ground states and first excited states using DMRG for systems with a ratio of the cylinder circumference to the magnetic length $L_y/l_B = 20$ and $N = 18$ LLL orbitals; additionally verifying with ED for $L_y/l_B = 8$ and $N = 8$. For the \mathbb{Z}_2 scenario with open boundary conditions, the first excited states are edge states described by a change in the total Chern number by -2 . From these first excited states, we show the gap grows as we stretch the cylinder from $L_y = 15l_B$ to $20l_B$ for the \mathbb{Z}_2 case, suggesting a true gap in the thermodynamic limit.

This paper is organized as follows: in section 1 we lay out an analytic argument for the ground state of the aforementioned (repulsive) interacting quantum Hall problems, \mathbb{Z}_2 and spin- $\frac{1}{2}$ QH; in section 2 we construct pseudopotentials for both scenarios by placing the problem onto a cylinder, which makes one direction compact and reduces the 2D continuum problem to an effective 1D discrete chain; following this, in section 3, we use DMRG

to solve for both the ground state manifolds of the constructed pseudopotentials and the system size scaling of the energy gap. In section 4, we study the nature of the excited states for smaller cylinders using ED, and show an interesting property of this model – product eigenstates at higher energy, the number of which grows with system size. We choose to use naturalized units such that $e = \hbar = c = 1$, the magnetic length is $l_B = B^{-1/2}$, and further set the mass of every particle to $m = 1$.

II. QUANTUM HALL POLARIZATION

When a uniform magnetic field B is applied to a sample of electrons, the sample can be understood to be “discretized” in the sense that the non-interacting single-particle states, i.e Landau levels, take on an integer degeneracy (not including spin or flavour) N which is equal to the division of the sample area A by the area of the quantized cyclotron orbit $2\pi l_B^2$. As the magnetic field is increased, the area of the quantized cyclotron orbits shrinks, both driving up the degeneracy of the Landau levels and increasing the energy gap between them [30, 32, 34]. Naturally, electronic interactions would intermix these single-particle states; however, if the magnetic field is large enough, the resulting gap between different energy Landau levels may dominate over the electron-electron interactions, preventing Landau level mixing. Thus, in the presence of a strong enough magnetic field, the interacting many-body ground state of a partially or fully occupied lowest Landau level can be described without the need for higher Landau levels [30, 31, 34].

Given a large enough magnetic field, non-interacting electrons occupy a discrete set of LLL orbitals; therefore, a natural question to ask is: How does the filling, or number of electrons in the sample, affect the ground state in the presence of strong repulsive interactions? At $\nu = 1$, it is possible to place one particle per LLL orbital. Since the Landau-gauge orbitals are localized in at least one direction, and repulsive interactions naturally drive particles apart, one might expect that at $\nu = 1$, the ground state would be just one particle per LLL orbital. As that configuration minimizes the energy by separating the repelling particles as far as possible.

When electrons have no spin or additional flavour, the above scenario is fully filled and trivial; however, if the electrons have spin, it has been long understood that the repulsive interactions form a ferromagnet [34], often referred to in literature as the half-filled or $\nu = 1$ ferromagnet ($\nu = 2$ being fully filled) [36].

Here we prove mathematically, following similar variational arguments in Ref [10, 17], that a ground state of the spin- $\frac{1}{2}$ system at this filling is indeed one particle per site, and completely spin-polarized. To start, we note that it is implied that the single-particle annihilation operator at position $\mathbf{r} = (x, y)$ within the sample area can be expanded in terms of all Landau level wavefunctions

$\psi_a(x, y|m)$ – with increasing energy labelled by index a , spin $\beta \in \{\uparrow, \downarrow\}$, and Landau level orbital m – as

$$c_\beta(\mathbf{r}) = \sum_{a=0}^{\infty} \sum_m \psi_a(x, y|m) d_{\beta, a, m}. \quad (1)$$

The Hamiltonian is $H = \hat{T} + \hat{V}$, where the kinetic energy \hat{T} is diagonal in the Landau level single-particle basis Eqn 1, and can be decomposed into sum of contributions from each Landau level $\hat{T} = \hat{T}_0 + \hat{T}_1 + \dots$. The difference between the lowest Landau level \hat{T}_0 and the first excited Landau level \hat{T}_1 is an important scale in this argument; we denote it as ω . In particular we are interested in the limit where the magnetic field is tuned such that the gap between Landau levels ω is much larger than the interaction strength, thus suppressing Landau level intermixing and making all single-particle states but the LLL prohibitively expensive for fermions to occupy. Following this requirement, we constrain our variational state $|\psi\rangle$ to the sector of Fock space describing many-body states formed out of single-particle LLL wavefunctions, killing all contributions from the kinetic energy \hat{T} except \hat{T}_0 . The latter being a constant which can be gauged away. We are now left with the task of minimizing the 2-body interaction operator \hat{V} , which is written

$$\hat{V} = \sum_{\mathbf{r} \mathbf{r}'} c_\alpha^\dagger(\mathbf{r}) c_\beta^\dagger(\mathbf{r}') V(\mathbf{r} - \mathbf{r}') c_\beta(\mathbf{r}') c_\alpha(\mathbf{r}). \quad (2)$$

However, at a commensurate filling, where it is possible to place the same number of particles per site, the density-density representation is more facilitating. One might simply anticommute the fermion annihilation and creation operators in order to place Eqn 2 into the density-density form minus a quadratic piece

$$\begin{aligned} \hat{V} &= \sum_{\mathbf{r} \mathbf{r}'} c_\alpha^\dagger(\mathbf{r}) c_\alpha(\mathbf{r}) V(\mathbf{r} - \mathbf{r}') c_\beta^\dagger(\mathbf{r}') c_\beta(\mathbf{r}') \\ &- V(0) \sum_{\mathbf{r}} c_\alpha^\dagger(\mathbf{r}) c_\alpha(\mathbf{r}). \end{aligned} \quad (3)$$

In thermodynamic limit, the quadratic piece is a global constant and can be neglected (see Supplement-B). Thus, the ground state can be determined by minimizing the interaction in the density-density form, which we henceforth call H' . We take H' into the momentum basis and act it on our variational state:

$$H' |\psi\rangle = \sum_{\mathbf{q}} \hat{n}(\mathbf{q}) \tilde{V}(\mathbf{q}) \hat{n}(-\mathbf{q}) |\psi\rangle, \quad (4)$$

where $\hat{n}(\mathbf{q}) = \sum_{\mathbf{r}} e^{i\mathbf{q} \cdot \mathbf{r}} \hat{n}(\mathbf{r})$ is the Fourier transform of the density operator. Writing this operator in the momentum basis has a two-fold purpose. First, since $\hat{n}(-\mathbf{q})^\dagger = \hat{n}(\mathbf{q})$ in the momentum basis, the above becomes

$$= \sum_{\mathbf{q}} |\hat{n}(\mathbf{q})|^2 \tilde{V}(\mathbf{q}) |\psi\rangle,$$

which is the sum of positive semi-definite functions of \mathbf{q} (i.e for non-zero values of the hermitian operator $|\hat{n}(\mathbf{q})|^2$ and $\tilde{V}(\mathbf{q}) \geq \tilde{V}(0) \geq 0$). Thus every term with a non-zero value of $|\hat{n}(\mathbf{q})|^2$ increases the total interaction energy. Secondly, in the momentum basis the density operator is a sum over terms quadratic in the fermion operators: $n_{\mathbf{q}} = \sum_{\mathbf{k}} c_{\alpha}^{\dagger}(\mathbf{k} + \mathbf{q})c_{\alpha}(\mathbf{k})$. When such an operator is acted onto a state which is one particle per orbital, and all the same flavour (i.e spin polarized up $|\uparrow\uparrow\cdots\uparrow\rangle$ or down $|\downarrow\downarrow\cdots\downarrow\rangle$), all but the $\mathbf{q} = 0$ terms vanish. Thus, $|\psi\rangle$ chosen to be flavour polarized with one particle per orbital minimizes the Hamiltonian, as the sum of positive semi-definite terms collapses to a single term:

$$= |\hat{n}(0)|^2 \tilde{V}(0) |\psi\rangle.$$

Thus the ground state is one without exchange between single-particle orbitals. Remembering that a large gap ω places a prohibitive energy cost to occupying higher Landau levels than LLL, so the true ground state $|\psi\rangle$ must be one which is one particle per LLL orbital and polarized. These two fully polarized states are not the only states in the ground state manifold [36], which (for an N -particle system) includes $N - 1$ additional states which are eigenstates of S^2 with eigenvalue $\frac{N}{2}(\frac{N}{2} + 1)$. These are those states which are connected to a fully polarized states by the total spin raising and lowering operator S_{\pm} . One might imagine that other eigenstates of S^2 might be solutions to the Hamiltonian (2), however, different irreducible representations of the $SU(2)$ symmetry (i.e different eigenstates of S^2 with eigenvalues less than $\frac{N}{2}(\frac{N}{2} + 1)$) are not connected by any such operation, and thus there is no requirement for them to be the same energy as those states in the ground state manifold.

If one were to substitute this system of spin- $\frac{1}{2}$ fermions in a magnetic field B with one which is spinless, but which includes Landau levels with opposite magnetic fields $\pm B$ (i.e \mathbb{Z}_2), then the language of the argument would still hold, thus demanding that the ground state manifold contain two states: one fermion per LLL of type $+B$, which we write $|+\cdots+\rangle$, and its \mathbb{Z}_2 partner $|-\cdots-\rangle$. As will be discussed in the following section, unlike the $\nu = 1$ spin- $\frac{1}{2}$ QH, the \mathbb{Z}_2 scenario has no additional states, owing to its reduced symmetry.

III. PSEUDOPOTENTIALS: FROM 2D TO 1D

Due to the uniform nature of the magnetic field, the underlying spatial symmetries of the sample – translational and rotational – are preserved. Therefore degenerate single-particle states are necessarily labelled, up to a choice of gauge, by the eigenvalues of their generators. The choice of gauge is unphysical and arbitrary, thus choosing a gauge which preserves translational symmetry in one direction, the Landau gauge [32], gives rise to a spectrum composed of degenerate manifolds of single-particle states labelled by momentum in one direction

(say k_y). If we impose periodic boundary conditions in the y -direction, by wrapping our sample of area A into a cylinder of circumference L_y , the centers of localization become uniformly spaced with incremental values of $l_B^2 k_y = \frac{l_B^2}{L_y} 2\pi n$; where $n \in \mathbb{Z}$ for an odd number of sites N and $n \in \mathbb{Z} + \frac{1}{2}$ for even N [33]. With this choice of geometry, adiabatically threading a flux quantum through the loop of the cylinder moves the center of a Landau level wavefunction into its neighbor's [35, 45]. The direction ($\pm \hat{x}$) in which the wavefunctions evolve depends on the sign of the magnetic field, with opposite magnet field Landau level centers evolving in opposite directions. We make this explicit in defining the LLL wavefunction [16], which we write (up to a normalization \mathcal{N}):

$$\phi_{\xi, k_y}(\mathbf{r}) = \mathcal{N} \exp\left(iy k_y - \frac{1}{2l_B^2}(x - \xi l_B^2 k_y)^2\right), \quad (5)$$

where $\xi = \pm 1$ indicates the sign of the magnetic field, i.e the Chern number of the LLL. By restricting the electrons to occupy only the LLL's, we obtain a picture reminiscent of a 1D chain (Fig 2), except where the chain “sites” label different degenerate single-particle LLL's of increasing momentum k_y . Practically, this projection is done by defining the LLL-projected electron operator

$$\hat{c}_{\alpha}(\mathbf{r}) = \sum_{\xi, n} \phi_{\xi, k_y}(\mathbf{r}) d_{\alpha, \xi, n}, \quad (6)$$

which replaces $c_{\alpha}(\mathbf{r})$ in Eqn 2. The LLL operator $d_{\alpha, \xi, n}$ destroys a fermion with spin $\alpha \in \{\uparrow, \downarrow\}$, sign of magnetic field ξ , and momentum $k_y = \frac{2\pi n}{L_y}$.

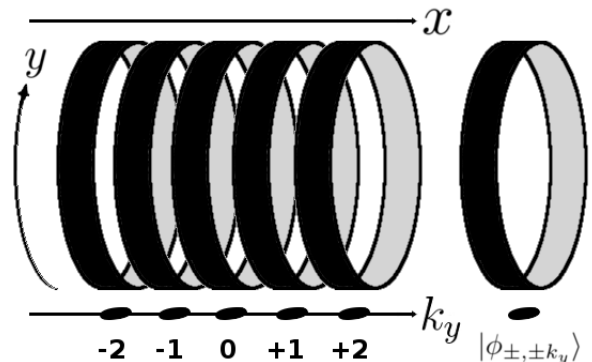


FIG. 2. The cylindrical sample of area $A = L_x L_y$ and circumference L_y , subdivided according to the LLL wavefunction centers which form the corresponding chain of LLL orbitals.

Naturally, the form of the interaction \hat{V} upon projection depends on the problem: spin- $\frac{1}{2}$ QH or \mathbb{Z}_2 . In the spin- $\frac{1}{2}$ case, all fermions feel the same sign of the magnetic field $\xi = +1$. Dropping the redundant label, the projected interaction is

$$H_{\frac{1}{2}\text{QH}} = \sum_{n, k, m} V_{km} d_{\alpha, n+k}^{\dagger} d_{\beta, n+m}^{\dagger} d_{\beta, n+m+k} d_{\alpha, n}, \quad (7)$$

where n are integers (half-integers) if the number of sites is odd (even), and $k, m \in \mathbb{Z}$ always [33]. The matrix elements for a general projected two-body interaction are

$$V_{km} = \sum_{\tilde{x}\tilde{y}} V(\tilde{x}, \tilde{y}) e^{-i\tilde{y}\frac{2\pi k}{L_y}} e^{-\frac{1}{2l_B^2}(\tilde{x}+l_B\frac{2\pi m}{L_y})^2} e^{-\frac{1}{2}l_B^2(\frac{2\pi k}{L_y})^2} \quad (8)$$

with $(\tilde{x}, \tilde{y}) \equiv (\mathbf{r} - \mathbf{r}')$.

Turning now to our toy model for TBG, where the opposite magnetic field LLL's are analog to the gauge-fixed hybrid Wannier states [16, 40, 41] in the chiral limit [15, 18]. For simplicity, we polarize the spin (and make it effectively spinless). We therefore drop the redundant spin index, and find the projected interaction to be

$$\begin{aligned} H_{\mathbb{Z}_2} = & \sum_{n,k,m} V_{km} \left(d_{+,n+k}^\dagger d_{+,n+m}^\dagger d_{+,n+m+k} d_{+,n} \right. \\ & + d_{-,-n}^\dagger d_{-,-n-m-k}^\dagger d_{-,-n-m} d_{-,-n-k} \quad (9) \\ & \left. + 2d_{+,n+k}^\dagger d_{-,-n-m-k}^\dagger d_{-,-n-m} d_{+,n} \right), \end{aligned}$$

where V_{km} is likewise Eqn 8. By inspection, one can see that Eqn 9 conserves Chern number – a consequence of the sublattice polarization in the CSCM (Scenario 2 introduced in Introduction). Just as with the spin- $\frac{1}{2}$ QH Hamiltonian Eqn 7, only two flavours of fermions are present, except here the $SU(2)$ symmetry is reduced to the \mathbb{Z}_2 symmetry [24]. Following the argument laid out in Sec II, one ground state must be Chern polarized and one particle per LLL orbital: $|++\dots+\rangle$. It is straightforward to check if the polarized state is an eigenstate of the projected Hamiltonian:

$$\begin{aligned} H_{\mathbb{Z}_2} |++\dots+\rangle = & \quad (10) \\ & \sum_{|n|\leq Q, |n+k|\leq Q} \left(-V_{k,0} + V_{0,k} \right) |++\dots+\rangle, \end{aligned}$$

noting that $Q \equiv (N-1)/2$ is the magnitude of the edge orbital momentum; but it is not so obvious that this is the lowest energy state. For that we implement DMRG and solve Eqn 9 numerically for the screened Coulomb interaction (in the next section):

$$V_{sc}(\tilde{x}, \tilde{y}) = \frac{1}{\sqrt{\tilde{x}^2 + \tilde{y}^2}} \exp\left(-\frac{\sqrt{\tilde{x}^2 + \tilde{y}^2}}{l_s}\right). \quad (11)$$

However interesting, there is a special case which can be shown exactly – short-range contact-like interactions, $V_\delta(\tilde{x}, \tilde{y}) = \delta(\tilde{x})\delta(\tilde{y})$. We say “contact-like” because it treats inter-sublattice scattering as scattering at a point, which can be understood as a highly-screened Coulomb interaction. For this choice of interaction, the matrix element Eqn 8 becomes symmetric, i.e $V_{km} = V_{mk}$, and thus by Eqn 10, the energy of the polarized state is zero, as expected since like-flavour fermions are forbidden by Pauli exclusion from sharing their position. Conveniently, this choice of interaction is mathematically simpler to study than the screened Coulomb interaction, with the ground state of the repulsive interacting problem clearly marked by zero energy.

IV. DMRG

Mixed real-momentum space representations of the cylinder geometry, where the momentum in y -direction is used as a conserved quantum number, while keeping the locality in the x -direction, have been shown to greatly reduce the required computational time and memory for employing DMRG [48]. The non-trivial topology of the LLL takes this a step farther, tying together the position and momentum via a single quantum number (k_y), and effectively collapsing the problem down to a 1D system [33, 45].

Such approaches are well motivated for QH by exact Matrix Product State (MPS) representations discovered for QH systems – including the Laughlin, Moore-Read [50], and Haldane-Rezayi states [51] – and have been used to numerically calculate and characterize fractional QH states [42, 43, 45].

Unlike fractional QH ground states, the ground states of Eqn 7 and Eqn 9 at *integer* filling are much simpler. This is because they have a bond dimension which is equal to 1 for the fully polarized states, and scales linearly with the system size for those states of Eqn 7 connected to the polarized states by symmetry.

While the dimensional reduction of the QH problem in this guiding-center representation is computationally less costly, it comes at the cost of longer range (Gaussian localized [45]) interactions in the effective 1D picture, even for short range interactions in real space, e.g contact-like $V_\delta(\tilde{x}, \tilde{y})$. The range of these Gaussian localized interactions grows with the ratio L_y/l_B , therefore, if the number of orbitals in the x -direction is not large enough, one risks modifying the form of the interaction by its truncation due to the system size [42]. However, so long as there is one particle per every available LLL orbital, we find that the total number of LLL orbitals appears to have little to no effect on the ground state manifold. This peculiarity could be explained by the general nature of the argument in Sec II, which necessitates a polarized ground state so long as the repulsive interactions can be decomposed into a sum of positive semi-definite terms, and is otherwise independent of the shape of the interaction.

In order to better understand the system size scaling, and additionally to check for the presence of a gap, we used DMRG to determine the first excited states. We then plot the gap as a function of increasing number of orbitals, and find that it saturates at a fixed cylinder circumference. For the \mathbb{Z}_2 LLL's, increasing the cylinder circumference increases the saturation of the gap (Fig 3), thus suggesting that the gap remains in the thermodynamic limit.

The states which make up its first excited state manifold are well described by the trial state

$$|\psi\rangle_Q = d_{-,-Q}^\dagger d_{+,Q} |++\dots+\rangle, \quad (12)$$

where Q is the momentum index of the edge orbital, as well as those states related to it by the \mathbb{Z}_2 symmetry.

Eqn 12, which itself is an exact excited state (though at a higher energy), has total Chern number two less than the fully polarized state, i.e $N - 2$. Because the negative-Chern number LLL's have their guiding centers inverted about the origin relative to their positive-Chern counterparts (see Fig 7), the operator $d_{-,Q}^\dagger d_{+,Q}$ flips both the Chern number and momentum of the fermion at the (real-space) edge of the cylinder. The true lowest excited states determined by DMRG are similar, save for having the mode entangled amongst a few orbitals near the edge, rather than solely existing at the edge orbitals.

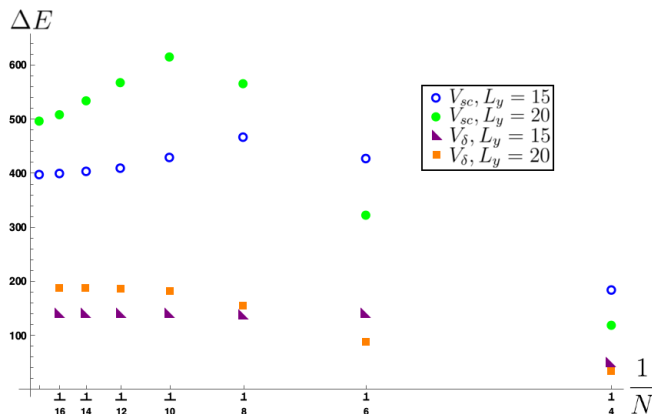


FIG. 3. Gap between ground and first excited state manifold for $H_{\mathbb{Z}_2}$ ($\nu = 1$) with contact-like and screened Coulomb interactions ($l_s = 1$), and each with different cylinder circumferences L_y , versus the total number of LLL orbitals N (and with $l_B = 1$). For a given L_y , a large enough N is necessary for the gap to tend toward saturation. The contact-like interaction doesn't suffer from the additional finite-size effects as does the longer-ranged screened Coulomb interaction, and consequently the gap saturates more quickly. Given either interaction, the gap saturation value increases as we increase the cylinder circumference.

For $H_{\frac{1}{2}\text{QH}}$, we use DMRG and converge to all $N + 1$ states in the ground state manifold, which includes both fully polarized states, and those connected by the symmetry S_{\pm} . As expected analytically, the ground state manifold is an irreducible representation of the $SU(2)$ symmetry, in particular, the eigenstates of S^2 with eigenvalue $\frac{N}{2}(\frac{N}{2} + 1)$. Just as with the ground states, the excited state manifold is an irreducible representation of the $SU(2)$ symmetry, except with eigenvalue $\frac{N-2}{2}(\frac{N-2}{2} + 1)$. Unlike Eqn 12, the change in spin is not strictly localized to the edge, and the gap appears to shrink with increasing cylinder circumference (Fig 4), which may suggest a spin-wave in the thermodynamic limit [34]; the study of which we leave for future research.

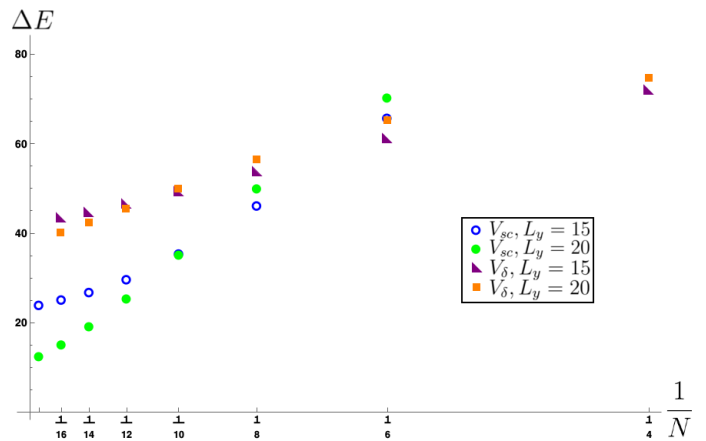


FIG. 4. Similar to Fig 3 but for $H_{\frac{1}{2}\text{QH}}$ ($\nu = 1$): gap between ground and first excited state manifold, plotted as $(\Delta E)^{-1}$, for contact-like and screened Coulomb interactions ($l_s = .3$), and each with different cylinder circumferences L_y , versus the total number of LLL orbitals N (and with $l_B = 1$). Unlike the \mathbb{Z}_2 case (Fig 3), the spin- $\frac{1}{2}$ QH at $\nu = 1$ exhibits a gap to the first excited state manifold which appears to shrink with increasing system size.

V. EXCITED STATES AND EMERGENT SPIN PHYSICS

Despite the numerical advantage afforded by the Landau gauge, the resulting projected Hamiltonian is by no means trivial. For starters, the kinetic energy is implicit in the construction of the model from the projection onto the LLL; and likewise, the Hamiltonian Eqn 9 is no simple sum of local density operators, instead bearing a non-trivial structure with correlated “hopping” across the chain of orbitals, which is deeply related to the momentum conservation around the cylinder. As such, one might not expect the ground state to be a product state, yet as we discussed in Sec II and shown numerically, product states are a natural consequence of strong interactions in these systems at integer filling. Given that these are truly two-dimensional systems, one would expect the entanglement in the ground state to at least follow area law, and scale linearly with the system size; and this indeed is the case for the states (except the polarized states) in the ground state manifold of the $SU(2)$ QH ferromagnet. However, when the symmetry is reduced to \mathbb{Z}_2 , the only states in the ground state are the polarized states, and thus area law appears to be beaten. Likewise, there exist excited product states, such as the edge state Eqn 12, which might exhibit better than area law scaling.

It is then natural to ask if excited states exist throughout the spectrum, what their fraction to dimension of the Hilbert space is, and if the number of those states increases with the system size. In order to answer these questions, we constrained ourselves to contact interactions on smaller cylinders and employed ED. We found

that the number of states with inverse participation ratio, $P_\alpha = \sum_n |\psi_{\alpha n}|^4$ for eigenstate ψ_α , with $P_\alpha > 0.95$ increases with the system size (Fig 5), but with a shrinking fraction compared to the total number of states (Fig 6). The latter suggests a connection of the product eigenstates to the open boundary conditions at the edge.

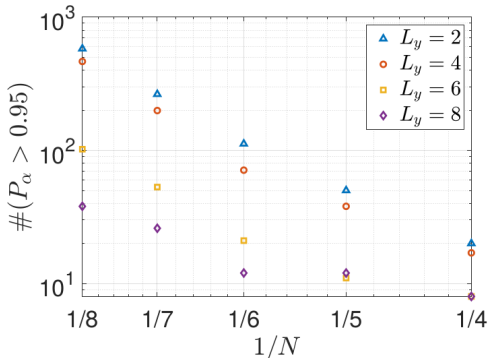


FIG. 5. The number of states with inverse participation ratio $P_\alpha > 0.95$ as a function of system size.

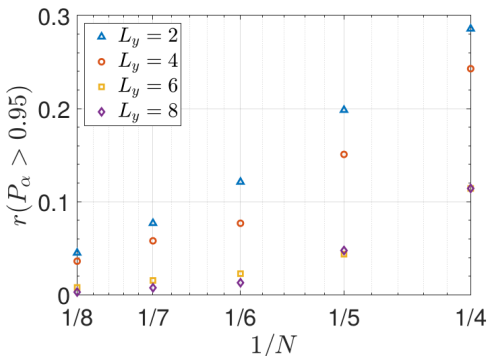


FIG. 6. The ratio of the number of states with inverse participation ratio $P_\alpha > 0.95$ to the dimension of the Hilbert space, as a function of system size.

The exact nature of the excited states found via ED suggests an interesting connection to 1D Ising-type spin physics, with Chern number playing the role of spin. As a prerequisite to making this connection, remember that because the real-space guiding centers of the opposite-Chern LLL's wind in opposite directions about the cylinder, a Chern $C = \pm 1$ Landau orbital at $\pm n$ are located together in real space, both having Gaussian centers at $x = 2\pi n l_B^2 / L_y$ (see Fig 7). Following this, we consider each LLL orbital with $C = \pm 1$ at momentum $\pm n$ to act as a *local* (in real space) spin, mapped to local spin states as: $|+\rangle_{+n} \rightarrow |\uparrow\rangle_n$ and $|-\rangle_{-n} \rightarrow |\downarrow\rangle_n$. Each is an eigenstate of the local Pauli-Z Chern-pseudospin operator

$$Z_n = \frac{1}{2} \left(d_{+,n}^\dagger d_{+,n} - d_{-,-n}^\dagger d_{-,-n} \right) \quad (13)$$

with eigenvalue $\pm 1/2$. For example, Eqn 12 for $N = 4$,

$$d_{-,2}^\dagger d_{+,-2} |++++\rangle = |0, +, +, \pm\rangle,$$

corresponds to the many-body spin state $|\downarrow, \uparrow, \uparrow, \uparrow\rangle$. Understandably, since the electrons are not fixed spins, and double occupancy of orbitals with the same real-space guiding centers can occur, there exists states in the Fock space, such as $|-, +, +, +\rangle$, where $Z_{\pm 2} = 0$ and therefore do not have a corresponding local-spin state. Since states which do not follow this scheme necessarily have electrons at the same guiding center, they are guaranteed, because of the repulsive interactions, to be at a high energy than those with non-zero eigenvalues of Z_n .

This apparent correspondence between the low energy product states and local spin moments motivates a different way of thinking about the model as a whole, where intuition about 1D models of local moments, such as the Ising model, translates into something physically meaningful in the 2D \mathbb{Z}_2 QH problem. In the Supplementary-F, we detail how the Ising transverse field $\sum_i h X_i$, which pushes the spins into the xy-plane, corresponds (to leading order in l_B/L_y) to a wall defect along the length of the cylinder in real space. Since opposite-Chern LLL with the same real-space center move in opposite directions about the cylinder, the largest contribution to colliding with the wall is to flip the Chern number at that guiding center, thus mixing the “spin”. We do not explore the consequences of such a term to ground state physics, nor explore this correspondence beyond what we have discussed here, as this moves beyond the scope of this paper, and instead leave this for future research.



FIG. 7. Density of the LLL's (Eqn 5) with $\xi = \pm 1$ in orbital $k_y = \pm 6 \frac{2\pi}{L_y}$. Opposite Chern LLL share the same guiding-center so long as they have opposite momentum. Cylinder circumference is $L_y/l_B = 15$, with $N = 18$ LLL orbitals.

VI. CONCLUSION

The recent advances in stacked 2D materials, including TBG, have opened an entirely new avenue for research into the interplay of topology and strong interactions, only previously possible with metals in high magnetic fields. In this paper, we provide a simple model, constructed out of continuum lowest Landau levels, which

captures the essential physics of two strongly interacting flat bands when the bands have identical ($H_{\frac{1}{2}\text{QH}}$) or opposite ($H_{\mathbb{Z}_2}$) Chern number, and we study it at integer filling. We find for either problem, that the ground state is a fully-polarized state (or symmetry related). Let us take the opposite spins of the spin- $\frac{1}{2}$ QH problem to represent opposite layers of the bilayer QH problem. If we introduce an inter-layer interaction anisotropy which bias one layer over another, the $SU(2)$ symmetry breaks, splitting the extensive degeneracy of the ground state manifold and selecting out a spin(layer)-coherent ground state (see Supplementary-E). Such an instability toward a coherent state does not exist for repulsion between bands of opposite Chern number, where the ground state is only two-fold degenerate between spontaneously \mathbb{Z}_2 -symmetry broken states [24], and appears to be separated by a gap from the rest of the spectrum. These results are in agreement with mean field theory [16] and provide a simple explanation for the stability of a Chern-polarized ground state.

In order to study this problem numerically, we rolled our 2D sample into a cylinder geometry and constructed pseudopotentials by projecting our interactions onto the LLL in the Landau gauge. We used ED to verify the ground state for small cylinders; and using DMRG, we found the ground states in agreement with ED and analytics (Sec II). In addition, we calculated the gap to the first excited states, and showed the gap increases as we stretch the cylinder from $L_y = 15l_B$ to $20l_B$ for the \mathbb{Z}_2 scenario. For the spin- $\frac{1}{2}$ QH case, the gap appears to shrink with increasing system size.

The primary purpose of this paper is to provide a simple model for the study of strongly interacting problems in electronic systems with non-trivial topological bands and net-zero Chern number. More broadly, this work is meant to inspire further study [18] of crystals with topologically non-trivial Chern bands. In these scenarios, one can take advantage of the fact that it is always possible to construct maximally localized functions in 1D, and by extension, a gauge can be chosen in 2D such that single-particle wavefunctions are maximally localized along one direction [16, 40]. As with the LLL wavefunction, the real-space centers of these hybrid Wannier states are adiabatically connected through increasing/decreasing momenta, and thus there exists a dimensional reduction from 2D to 1D advantageous to numerics. Original constructions for such single-particle states [40] suffered from a gauge freedom which made the practical description of many-body states, such as the lattice analog to the FQH, impossible – plagued by insignificant overlaps between exact FQH ground states on a lattice and those constructed from the Laughlin wavefunction using hybrid Wannier states [41]. This was later remedied by *Wu, Regnault, and Bernevig* [41] through a procedure which trades off exact 1D maximal localization for exponential localization, but produces an orthonormal basis which

can be gauge-fixed such that they behave like Landau orbitals. Very recently, such gauge-fixed hybrid Wannier states for Chern bands have been used to study strong interactions in TBG [18]. In general, this approach allows a more natural study of the MHS, capturing those details, such as a finite bandwidth and detailed shape of the Wannier functions, not available to the LLL.

Part of the success of this DMRG technique applied to the models studied here is in part due to the low bond dimension of the ground states, which was true independent of our choice of interaction. This is in large part due to the preference of the repulsive interactions to choose a state which suppresses inter-orbital scattering, when the filling is such that one particle can be placed per single-particle orbital (i.e an integer filling). It may be that such low bond-dimension ground and excited states are more general to strongly repulsive systems at integer filling, which would make these numerical approaches an invaluable tool in the exploration of the plethora of new devices hosting topologically non-trivial narrow bands, as well as studying interacting QH states, such as the $\nu = 1$ QH ferromagnet [34, 36] studied here. This could include extending our study of the $\nu = 1$ QH state by including bilayer-type anisotropies or Zeeman terms not included in Eqn 7, which would provide a fertile platform for studying exciton condensation in bilayer devices [36, 37] or probing the lowest energy excitations of the $\nu = 1$ QH [34]. And additionally, the \mathbb{Z}_2 LLL's may open up a pathway toward testing recently proposed connections between \mathbb{Z}_2 topological order, thermalization, and information scrambling in two-dimensions [52, 53].

As a final point, if one were to introduce a single-particle potential to Eqn 9 which biases one Chern-flavour over the other, then in the limit where one flavour electron is prohibitively expensive to create, Eqn 9 reduces to the pseudopotentials for the well known spin-polarized QH [48]. Thus at fractional filling $\nu = 1/3$ there exists the famous FQH state well-described by the Laughlin wavefunction [20, 35]. Seeing that in TBG, no zero-field FQH state has yet been observed, it is an interesting question to ask what is the fate of the FQH at $\nu = 1/3$ when the bias is taken to be zero, i.e approaching \mathbb{Z}_2 .

VII. ACKNOWLEDGEMENTS

We would like to thank Jian Kang and Kai Sun for helpful discussion, and we are especially thankful to Oskar Vafeek for his invaluable insight and many helpful discussions. P. Myles Eugenio is supported by NSF DMR-1916958. Ceren B. Dağ is supported by NSF Grant EFRI-1741618. The DMRG calculations performed here used the Intelligent Tensor C++ library (version 2.0.11) [54].

-
- [1] Y. Cao, et al. *Nature* 556, 80-84 (2018)
- [2] A. L. Sharpe, et al. *Science* Vol 365, Issue 6453, pp 605-608 (2019)
- [3] M. Serlin, et al. arXiv:1907.00261 (2019)
- [4] Y. Cao, et al. *Nature* 556, 43-50 (2018)
- [5] M. Yankowitz, et al. *Science* Vol. 363, Issue 6431, pp. 1059-1064 (2019)
- [6] Yonglong Xie, et al. *Nature* 572, 101 (2019).
- [7] Dillon Wong, et al. arXiv:1912.06145 (2019).
- [8] R. Bistritzer and A. H. MacDonald. *PNAS* 108 (30) 12233-12237 (2011)
- [9] J. Kang and O. Vafek. *Phys Rev X* 8, 031088 (2018)
- [10] J. Kang and O. Vafek. *Phys Rev Lett* 122, 246401 (2019)
- [11] J. W. F. Venderbos and R. M. Fernandes. *Phys Rev B* 98, 245103 (2018)
- [12] L. Zou, H.C. Po, A. Vishwanath, T. Senthil. *Phys Rev B* 98, 085435 (2018)
- [13] Jianpeng Liu, Junwei Liu, and Xi Dai. *Phys Rev B* 99, 155415 (2019)
- [14] T. Hazra, N. Verma, M. Randeria. arXiv:1811.12428v2 (2018)
- [15] G. Tarnopolsky, A. J. Kruchkov, and A. Vishwanath. *Phys Rev Lett* 122, 106405 (2019)
- [16] N. Bultinck, S. Chatterjee, M. P. Zaletel. *Anomalous Hall ferromagnetism in twisted bilayer graphene*. arXiv:1901.08110 (2019)
- [17] C. Repellin, Z. Dong, Y. Zhang, and T. Senthil. *Ferromagnetism in narrow bands of moiré superlattices*. arXiv:1907.11723 (26 July 2019)
- [18] Jian Kang and Oskar Vafek. arXiv:2002.10360 (2020)
- [19] Xiaoyu Wang and Oskar Vafek. arXiv:2002.02057 (2020)
- [20] Patrick J Ledwith, Grigory Tarnopolsky, Eslam Khalaf, Ashvin Vishwanath. arXiv:1912.09634 (2019)
- [21] Nick Bultinck, Eslam Khalaf, Shang Liu, Shubhayu Chatterjee, Ashvin Vishwanath, Michael P. Zaletel. *Ground State and Hidden Symmetry of Magic Angle Graphene at Even Integer Filling*. arXiv:1911.02045 (2019)
- [22] N. Marzari, A. A. Mostofi, J. R. Yates, I. Souza, and D. Vanderbilt. *Rev Mod Phys* 84, 1419 (2012)
- [23] Philip W. Anderson. *Local Moments and Localized States*. Nobel Lecture, December 8, 1977.
- [24] Titus Neupert, et al. *Phys. Rev. Lett.* 108, 046806 (2012)
- [25] Ya-Hui Zhang, Dan Mao, Yuan Cao, Pablo Jarillo-Herrero, and T. Senthil. *Phys Rev B* 99, 075127 (2019)
- [26] B. L. Chittari, G. Chen, Y. Zhang, F. Wang, and J. Jung. *Phys Rev Lett* 122, 016401 (2019)
- [27] G. William Burg, et al. arXiv:1907.10106
- [28] Chen, G., Sharpe, A.L., Gallagher, P. et al. Signatures of tunable superconductivity in a trilayer graphene moiré superlattice. *Nature* 572, 215219 (2019)
- [29] Chen, G., Sharpe, A.L., Fox, E.J. et al. Tunable correlated Chern insulator and ferromagnetism in a moiré superlattice. *Nature* 579, 5661 (2020)
- [30] David Tong, *Lectures on the Quantum Hall Effect*. arXiv:1606.06687v2 (2016)
- [31] E. H. Rezayi and F. D. M. Haldane. *Phys Rev B* 50, 17199 (1994)
- [32] L. D. Landau and E. M. Lifshitz. *Quantum Mechanics Non-relativistic Theory, Course of Theoretical Physics, Vol 3*, 2nd edition, Pergamon (1965)
- [33] G. Ortiz, Z. Nussinov, J. Dukelsky, and A. Seidel. *Phys Rev B* 88, 165303 (2013)
- [34] Steven M. Girvin. *The Quantum Hall Effect: Novel Excitations and Broken Symmetries*. Topological Aspects of Low Dimensional Systems, ed. A. Comtet, T. Jolicœur, S. Ouvry, F. David (Springer-Verlag, Berlin and Les Editions de Physique, Les Ulis, 2000)
- [35] Robert B. Laughlin. *Fractional Quantization*. Nobel Lecture, December 8, 1998.
- [36] Kentaro Nomura and Daijiro Yoshioka. *Phys Rev B* 66, 153310 (2002)
- [37] H A Fertig and Ganpathy Murthy. *Advances in Condensed Matter Physics*, Vol 2011, Article ID 349362 (2010)
- [38] Alexey A. Soluyanov and David Vanderbilt. *Phys Rev B* 83, 035108 (2011)
- [39] Georg W. Winkler, Alexey A. Soluyanov, and Matthias Troyer. *Phys Rev B* 93, 035453 (2016)
- [40] Xiao-Liang Qi. *Phys Rev Lett* 107, 126803 (2011)
- [41] Yang-Le Wu, N. Regnault, and B. Andrei Bernevig. *Phys. Rev. B* 86, 085129 (2012)
- [42] E. J. Bergholtz and A. Karlhede. unpublished, arXiv:cond-mat/0304517v2 (2003)
- [43] Sonika Johri, Z Papic, P Schmitteckert, R N Bhatt, and F D M Haldane. *New Journal of Physics*, Volume 18, February 2016.
- [44] Zi-Xiang Hu, Z. Papic, S. Johri, R. N. Bhatt, Peter Schmitteckert. *Comparison of the density-matrix renormalization group method applied to fractional quantum Hall systems in different geometries*. arXiv:1202.4697 (2012)
- [45] Michael P. Zaletel, Roger S. K. Mong, and Frank Pollmann. *Phys Rev Lett* 110, 236801 (2013)
- [46] Michael P. Zaletel, Roger S. K. Mong, Frank Pollmann, and Edward H. Rezayi. *Phys. Rev. B* 91, 045115 (2015)
- [47] Ulrich Schollwöck. *Annals of Physics* 326, 96 (2011)
- [48] J. Motruk, M. P. Zaletel, R. S. K. Mong, and F. Pollmann. *Phys Rev B* 93, 155139 (2016)
- [49] Shouvik Sur, Shou-Shu Gong, Kun Yang, and Oskar Vafek. *Phys Rev B* 98, 125144 (2018)
- [50] Michael P. Zaletel and Roger S. K. Mong. *Phy Rev B* 86, 245305 (2012)
- [51] V. Crépel, N. Regnault, B. Estienne. arXiv:1905.05192 (2019)
- [52] Jack Kemp, Norman Y Yao, Christopher R Laumann, and Paul Fendley. *J. Stat. Mech.* (2017) 063105
- [53] Ceren B Dağ, L-M Duan, and Kai Sun. arXiv:1906.05241 (2019)
- [54] ITensor Library (version 2.0.11) <http://itensor.org>

VIII. SUPPLEMENTARY

A. Derivation of $H_{\mathbb{Z}_2}$

As discussed in the Introduction, there are two scenarios which inspire the study of TBG using LLL wavefunctions. Just as with the main text, we focus on, and use the language of the valley-polarized Scenario (2) in constructing the toy model. The valley-polarized Scenario (2) can be understood in analogy with the continuum model of TBG [8], where opposite-sign magnetic field LLL's play the role of opposite-sublattice hWS's in the chiral limit [18]. Thus, we construct this model using continuum LLL's [32]. Working in the Landau gauge [32], the LLL wave functions are

$$\phi_{\xi,k}(\mathbf{r}) = \mathcal{N} e^{iky} e^{-\frac{1}{2l_B^2}(x-\xi l_B k)^2}, \quad (14)$$

which are localized along the x -axis and compact about the cylinder's circumference (L_y) in y -direction. The (spinless/spin-polarized) projected single-particle annihilation operator is thus

$$\hat{c}(\mathbf{r}) = \sum_{k,\xi} \phi_{\xi,k}(\mathbf{r}) d_{\xi,k}, \quad (15)$$

where $d_{\xi,k}$ annihilates a fermion with sign of magnetic field $\xi = \pm 1$ at LLL orbital k , as described in Sec III. Opposite magnetic field LLL are defined to be on opposite sublattices at any given point \mathbf{r} , and orthogonal by construction. This leads us to consider only operators which necessarily conserve Chern number ξ , i.e

$$\sum_{\mathbf{r}} \hat{c}^\dagger(\mathbf{r}) f(\mathbf{r}) \hat{c}(\mathbf{r}) = \sum_{\xi} \sum_{kp} d_{\xi,k}^\dagger d_{\xi,p} \left(\sum_{\mathbf{r}} \phi_{n,k}^*(\mathbf{r}) \phi_{n,p}(\mathbf{r}) f(\mathbf{r}) \right). \quad (16)$$

Likewise, if instead we considered Scenario (1), the inverse Moire length scale l_M^{-1} is significantly smaller than the momentum-space separation between electronic states in opposite valleys a^{-1} (where a is the graphene lattice constant). Thus, for the long-range Coulomb interaction, scattering between valleys is highly suppressed relative to scattering within a valley [10, 16, 25], and as with Scenario (2), we need keep only Chern number conserving terms in the interaction. Whatever the case, we construct the pseudopotentials by projecting the interaction operator onto these chosen single-particle states:

$$\begin{aligned} & \sum_{\mathbf{r}\mathbf{r}'} : \hat{c}^\dagger(\mathbf{r}) \hat{c}(\mathbf{r}) V(\mathbf{r}-\mathbf{r}') \hat{c}^\dagger(\mathbf{r}') \hat{c}(\mathbf{r}') : \\ &= \sum_{mn} \sum_{k_y p_y k'_y p'_y} : d_{m,k_y}^\dagger d_{m,p_y} d_{n,k'_y}^\dagger d_{n,p'_y} : \left(\sum_{\mathbf{r}\mathbf{r}'} \phi_{m,k_y}^*(\mathbf{r}) \phi_{m,p_y}(\mathbf{r}) V(\mathbf{r}-\mathbf{r}') \phi_{n,k'_y}^*(\mathbf{r}') \phi_{n,p'_y}(\mathbf{r}') \right) \\ &= \sum_{k_y p_y k'_y p'_y} : d_{+,k_y}^\dagger d_{+,p_y} d_{+,k'_y}^\dagger d_{+,p'_y} : \left(\sum_{\mathbf{r}\mathbf{r}'} \phi_{+,k_y}^*(\mathbf{r}) \phi_{+,p_y}(\mathbf{r}) V(\mathbf{r}-\mathbf{r}') \phi_{+,k'_y}^*(\mathbf{r}') \phi_{+,p'_y}(\mathbf{r}') \right) \\ &+ \sum_{k_y p_y k'_y p'_y} : d_{-,k_y}^\dagger d_{-,p_y} d_{-,k'_y}^\dagger d_{-,p'_y} : \left(\sum_{\mathbf{r}\mathbf{r}'} \phi_{-,k_y}^*(\mathbf{r}) \phi_{-,p_y}(\mathbf{r}) V(\mathbf{r}-\mathbf{r}') \phi_{-,k'_y}^*(\mathbf{r}') \phi_{-,p'_y}(\mathbf{r}') \right) \\ &+ 2 \sum_{k_y p_y k'_y p'_y} : d_{+,k_y}^\dagger d_{+,p_y} d_{-,k'_y}^\dagger d_{-,p'_y} : \left(\sum_{\mathbf{r}\mathbf{r}'} \phi_{+,k_y}^*(\mathbf{r}) \phi_{+,p_y}(\mathbf{r}) V(\mathbf{r}-\mathbf{r}') \phi_{-,k'_y}^*(\mathbf{r}') \phi_{-,p'_y}(\mathbf{r}') \right), \quad (17) \end{aligned}$$

taking note of the normal ordering. It is not necessary to calculate all three matrix elements, as they are related to the first by symmetry. We use the fact that $\phi_{-,k}(\mathbf{r}) = \phi_{+,-k}^*(\mathbf{r})$, and find

$$\begin{aligned} &= \sum_{k_y p_y k'_y p'_y} : \left(d_{+,k_y}^\dagger d_{+,p_y} d_{+,k'_y}^\dagger d_{+,p'_y} + d_{-,-p_y}^\dagger d_{-,-k_y} d_{-,-p'_y}^\dagger d_{-,-k'_y} + 2 d_{+,k_y}^\dagger d_{+,p_y} d_{-,-p'_y}^\dagger d_{-,-k'_y} \right) : \\ &\times \sum_{\mathbf{r}\mathbf{r}'} \left(\phi_{+,k_y}^*(\mathbf{r}) \phi_{+,p_y}(\mathbf{r}) V(\mathbf{r}-\mathbf{r}') \phi_{+,k'_y}^*(\mathbf{r}') \phi_{+,p'_y}(\mathbf{r}') \right) \end{aligned}$$

Writing the sums over \mathbf{r} and \mathbf{r}' as an integral over center-of-mass (X, Y) and relative coordinates (\tilde{x}, \tilde{y}) , we find that the explicit form of the matrix element takes the form

$$\begin{aligned}
& \int d\mathbf{r} d\mathbf{r}' \phi_{+,k_y}^*(\mathbf{r}) \phi_{+,p_y}(\mathbf{r}) V(\mathbf{r} - \mathbf{r}') \phi_{+,k'_y}^*(\mathbf{r}') \phi_{+,p'_y}(\mathbf{r}') \\
&= \int dY e^{iY(-k_y + p_y - k'_y + p'_y)} \int dX d\tilde{y} d\tilde{x} e^{i\frac{\tilde{y}}{2}(-k_y + p_y + k'_y - p'_y)} V(\tilde{x}, \tilde{y}) \\
&\times \exp\left(-\frac{2}{l^2}\left(X - \frac{l^2}{4}(k_y + p_y + k'_y + p'_y)\right)^2\right) \\
&\times \exp\left(-\frac{1}{2l^2}\left(\tilde{x} + \frac{l^2}{2}(-k_y - p_y + k'_y + p'_y)\right)^2\right) \\
&\times \exp\left(-\frac{l^2}{8}(k_y - p_y + k'_y - p'_y)^2\right) \times \exp\left(-\frac{l^2}{8}(k_y - p_y - k'_y + p'_y)^2\right),
\end{aligned} \tag{18}$$

which explicitly depends only on two momenta, as the others vanish upon integrating over the center-of-mass coordinates. If we then choose the following coordinates:

$$\begin{aligned}
k_y &= \frac{2\pi}{L_y}(n + k) \\
p_y &= \frac{2\pi}{L_y}n \\
k'_y &= \frac{2\pi}{L_y}(n + m) \\
p'_y &= \frac{2\pi}{L_y}(n + m + k)
\end{aligned}$$

we get Eqn 8, up to a constant multiplier. It is important to note that the operators in Eqn 7 and Eqn 9 conserve momentum, which appears explicitly in Eqn 18 as a delta-function upon integrating over Y .

As a final point, note that opposite-sign magnetic field fermions are Kramer partners under C_2T , and that consequently the LLL guiding centers of the effective 1D chain (see Fig 2) are inverted about the origin relative to its Kramer partner's, such that the operators d_{+,k_y}^\dagger and $d_{-,-k_y}^\dagger$ both create an electron at $x = l_B^2 k_y$ but with opposite momenta.

B. The LLL-projected number operator \hat{N}

In Section II we discussed a variational argument for the ground states of the $\nu = 1$ spin- $\frac{1}{2}$ QH and \mathbb{Z}_2 . This argument is precedent upon the fact that the total number operator

$$\hat{N} = \sum_{\mathbf{r}} c^\dagger(\mathbf{r})c(\mathbf{r}) \tag{19}$$

is a global constant upon projection to an N -particle state of LLL's. For a finite cylinder of length L_x , and using Eqn 5 with $\xi = +1$ and normalization $\mathcal{N}^{-1} = \sqrt{L_y l_B \pi^{1/2}}$, the number operator becomes

$$\hat{N} = \mathcal{N}^2 L_y \sum_n d_{\alpha,n}^\dagger d_{\alpha,n} \left(\int_{-\frac{L_x}{2}}^{\frac{L_x}{2}} dx e^{-\frac{1}{i^{\frac{1}{2}} l_B} (x - 2\pi l_B^2 / L_y n)^2} \right). \tag{20}$$

If $L_x \rightarrow \infty$, then

$$= \sum_n d_{\alpha,n}^\dagger d_{\alpha,n} = N\mathbf{1}$$

as expected for the number operator. However, if we instead restrict the integral to finite L_x , then the projected number operator is momentum dependent, i.e depends on the index of the LLL orbital n . As a consequence, because of the connection between the real-space centers of the LLL and their momentum, the projected number operator would function as a potential which is weakest near the edge. However, this appears to be a consequence of the

normalization of the LLL \mathcal{N} , which is only a constant if derived in the $L_x \rightarrow \infty$ limit. If we instead choose to fix L_x to be finite, and normalize LLL orbitals at different n differently, i.e

$$\mathcal{N}_n^{-2} = L_y \int_{-\frac{L_x}{2}}^{\frac{L_x}{2}} dx e^{-\frac{1}{l_B^2}(x-2\pi l_B^2/L_y n)^2}, \quad (21)$$

then Eqn 20, with \mathcal{N} replaced by \mathcal{N}_n would indeed be proportional to unity. Essentially, the edge potential is a manifestation of the fact that \mathcal{N} is only constant when the LLL's are normalized over infinite length cylinders, and thus demanding a finite number of LLL orbitals N requires adding a confining potential [43]. Note that by adding a single-particle potential $U(x)$, which is $U(x) = 1$ for $|x| > L_x/2$, and $U(x) = 0$ otherwise, we find

$$\begin{aligned} \hat{N} + \hat{U} &= \mathcal{N}^2 L_y \sum_n d_{\alpha,n}^\dagger d_{\alpha,n} \left(\int_{-\frac{L_x}{2}}^{\frac{L_x}{2}} dx e^{-\frac{1}{l_B^2}(x-2\pi l_B^2/L_y n)^2} + \int_{-\infty}^{-\frac{L_x}{2}} dx e^{-\frac{1}{l_B^2}(x-2\pi l_B^2/L_y n)^2} + \int_{+\frac{L_x}{2}}^{+\infty} dx e^{-\frac{1}{l_B^2}(x-2\pi l_B^2/L_y n)^2} \right) \\ &= \mathcal{N}^2 L_y \sum_n d_{\alpha,n}^\dagger d_{\alpha,n} \int_{-\infty}^{\infty} dx e^{-\frac{1}{l_B^2}(x-2\pi l_B^2/L_y n)^2} = N \mathbb{1}. \end{aligned} \quad (22)$$

The need for the confining potential being particularly true for fluid states like the fractional QH [43]; however, we do not consider such a term for the integer filling states we study here, as the electronic ground state is well localized with one particle per orbital, and in full agreement with analytics.

C. Eigenstates and eigenenergies

For an N -orbital system with end momenta magnitude labelled by integer/half-integer Q , the ground state energy of the fully polarized state $E_{|+\dots+\rangle}$ is:

$$H_{\mathbb{Z}_2} |+\dots+\rangle = \sum_n \theta_{(|n|\leq Q)} \sum_k \theta_{(|n+k|\leq Q)} \left(-V_{k,0} + V_{0,k} \right) |+\dots+\rangle, \quad (23)$$

which is Eqn 10 with the constraints over the sums of n and k written explicitly as step functions. The trial state $|\psi\rangle = d_{-,-Q}^\dagger d_{+,Q} |+\dots+\rangle$ (Eqn 12) is an exact eigenstate with energy:

$$\begin{aligned} H_{\mathbb{Z}_2} |\psi\rangle &= \left(2 \left(\sum_{0\leq m\leq 2Q} V_{0,m} \right) - 2V_{0,0} \right. \\ &\quad \left. + E_{|+\dots+\rangle} - \left(\sum_{-2Q\leq k\leq 0} V_{0,k} - V_{k,0} \right) - \left(\sum_{0\leq k\leq 2Q} V_{0,k} - V_{k,0} \right) \right) |\psi\rangle, \end{aligned} \quad (24)$$

which, because of inversion symmetry of the 2-body interaction in Eqn 8, can be simplified to

$$= \left(2 \left(\sum_{0 < m \leq 2Q} V_{0,m} \right) + E_{|+\dots+\rangle} - \left(\sum_{-2Q \leq k \leq 2Q} V_{0,k} - V_{k,0} \right) \right) |\psi\rangle.$$

Both these formula – Eqn 23 and 24 – agree with numerics exactly, with such exactness owing to the low bond dimension (at $\nu = 1$) of the MPS representation of the eigenstates we calculate in this paper. In Fig 8 we plot the energy difference between the product state Eqn 12 and the entangled lowest excited state determined by DMRG, which shows the two excited states are separated by a gap.

D. Two-point correlations in real space and their correlation holes

Throughout this paper, we point to the real-momentum space connection of the Landau-gauge LLL wavefunctions, which provides a useful guiding-center representation where we can understand the LLL wavefunctions as forming an effective 1D lattice (Fig 2). However, one needs to be careful in thinking of the guiding-center chain as a literal lattice in real space. This being because the chain is indexed by the eigenvalues of momentum about the cylinder circumference – not position. It is only as a convenient consequence of the non-trivial topology that, say, the localized LLL wavefunction center at $x = 0$ evolves into its neighbor's center at $x = k_y l_B^2$ when its momentum is increased adiabatically by $+k_y$. (And likewise, moving in the opposite direction $-k_y$ for the LLL wavefunctions which feel

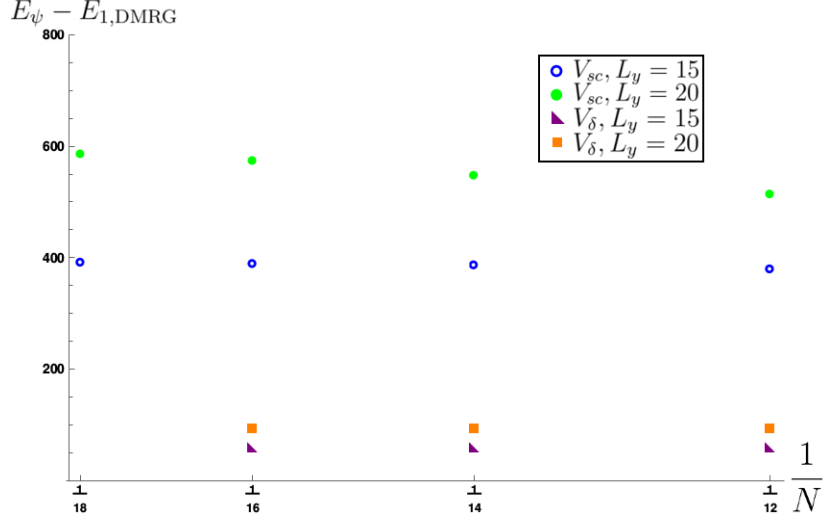


FIG. 8. Difference in energy between the trial eigenstate Eqn 12 (E_{ψ}) and the lowest excited state (E_1) determined by DMRG, showing a saturation to larger $E_{\psi} - E_1$ for larger cylinder circumferences. The screened Coulomb interaction length is $l_s = 1$, and magnetic length $l_B = 1$.

$B < 0$.) In truth, the LLL wavefunctions have non-zero amplitude everywhere on the cylinder (Eqn 5), such that (for example) Eqn 12 may have non-zero energy despite it being a product state in the guiding-center representation. This peculiarity of the Landau gauge, when not taken carefully, can misinform intuitive thinking, and thus one may need to resort to the real-space picture in order to fully understand a state's energetics.

For example, in the presence of contact interactions, the fully polarized ground state $|+\dots+\rangle$ has zero energy. This arising at the level of the projected interaction Eqn 8 as a symmetry of the matrix element $V_{km} = V_{mk}$, which generally forbids the like-Chern number electrons from interacting, and is additionally responsible for killing the energy of the polarized state. However, one might have immediately pointed out that such back flips are unnecessary, seeing that Pauli exclusion principle forbids same-flavour fermions from interacting at a point. Thus the fully polarized state, in spite of the wavefunctions overlapping in real space, must be at zero energy since it is composed of particles which are forbidden from interacting. More systematically, if we decompose the projected real-space annihilation operators into opposite-Chern components: $\hat{c}(\mathbf{r}) = \hat{c}_+(\mathbf{r}) + \hat{c}_-(\mathbf{r})$. The projected contact interaction reduces to a cross-term

$$= \sum_{\mathbf{r}} 2\hat{n}_+(\mathbf{r})\hat{n}_-(\mathbf{r}),$$

from which it follows that any state with only one flavour of fermion is a zero energy state.

This systematic approach can be expanded on by projecting the Hamiltonian onto the state

$$\begin{aligned} \langle +\dots+ | H_{\mathbb{Z}_2} | +\dots+ \rangle = \\ \iint d\mathbf{r} d\mathbf{r}' \langle +\dots+ | \hat{c}^\dagger(\mathbf{r})\hat{c}^\dagger(\mathbf{r}')\hat{c}(\mathbf{r}')\hat{c}(\mathbf{r}) | +\dots+ \rangle V(\mathbf{r}-\mathbf{r}'), \end{aligned} \quad (25)$$

and studying how the various correlations weight the expectation value of the state. For the fully polarized state, we only need to calculate a single correlation function:

$$\rho_0(\mathbf{r}, \mathbf{r}') = \langle +\dots+ | \hat{c}^\dagger(\mathbf{r})\hat{c}^\dagger(\mathbf{r}')\hat{c}(\mathbf{r}')\hat{c}(\mathbf{r}) | +\dots+ \rangle. \quad (26)$$

If, for a moment, we hold \mathbf{r}' fixed, then one may interpret $\rho_0(\mathbf{r}, \mathbf{r}')$ as the conditional probability of finding an electron at \mathbf{r} given an electron exists at fixed \mathbf{r}' . Now, if $\rho_0(\mathbf{r}, \mathbf{r}')$ is zero for some \mathbf{r} and \mathbf{r}' , having a ‘‘correlation hole’’ for the position of those two particles, then no energy $V(\mathbf{r}-\mathbf{r}')$ is contributed to the overall energy of the state. For a contact interaction, this means the state is zero energy. Since $|+\dots+\rangle$ is in the guiding-center representation, we can use Eqn 15 to find a closed form expression for ρ_0 . Doing so gives us (up to the normalization of the LLL wavefunction)

$$\begin{aligned} \rho(\mathbf{r}, \mathbf{r}') = \sum_{kk'pp'} \langle +\dots+ | d_{+,k}^\dagger d_{+,k'}^\dagger d_{+,p'} d_{+,p} | +\dots+ \rangle \\ \times e^{iy(-k_y+p_y)} e^{iy'(-k'_y+p'_y)} e^{-\frac{1}{2l^2}(x-l^2k_y)^2} e^{-\frac{1}{2l^2}(x-l^2p_y)^2} e^{-\frac{1}{2l^2}(x-l^2k'_y)^2} e^{-\frac{1}{2l^2}(x-l^2p'_y)^2}, \end{aligned} \quad (27)$$

where $k_y \equiv 2\pi k/L_y$. Writing $\langle \hat{O} \rangle_0 \equiv \langle + + \dots + | \hat{O} | + + \dots + \rangle$, this becomes

$$= \sum_{kk'pp'} \left(\langle d_{+,k}^\dagger d_{+,p} \rangle_0 \langle d_{+,k'}^\dagger d_{+,p'} \rangle_0 - \langle d_{+,k}^\dagger d_{+,p'} \rangle_0 \langle d_{+,k'}^\dagger d_{+,p} \rangle_0 \right) \\ \times e^{iy(-k_y+p_y)} e^{iy'(-k'_y+p'_y)} e^{-\frac{1}{2l^2}(x-l^2k_y)^2} e^{-\frac{1}{2l^2}(x-l^2p_y)^2} e^{-\frac{1}{2l^2}(x'-l^2k'_y)^2} e^{-\frac{1}{2l^2}(x'-l^2p'_y)^2},$$

and, using the constraints of quadratic correlation functions in the fully polarized state, further simplifies to

$$= \sum_{k,k'} e^{-\frac{1}{2l^2}(x-l^2k_y)^2} e^{-\frac{1}{2l^2}(x'-l^2k'_y)^2} \left(e^{-\frac{1}{2l^2}(x-l^2k_y)^2} e^{-\frac{1}{2l^2}(x'-l^2k'_y)^2} \right. \\ \left. - e^{i(y-y')(-k'_y+k_y)} e^{-\frac{1}{2l^2}(x'-l^2k_y)^2} e^{-\frac{1}{2l^2}(x-l^2k'_y)^2} \right).$$

Plotting this quantity (Fig 9) reveals a correlation hole for observing a $C = +1$ electron where a $C = +1$ electron already exists. Like-electrons in the presence of contact interactions never observe one another, forbidden by Pauli exclusion, which arises as the correlation hole, and thus a fully polarized state $|+ + \dots +\rangle$ is effectively non-interacting and zero-energy.

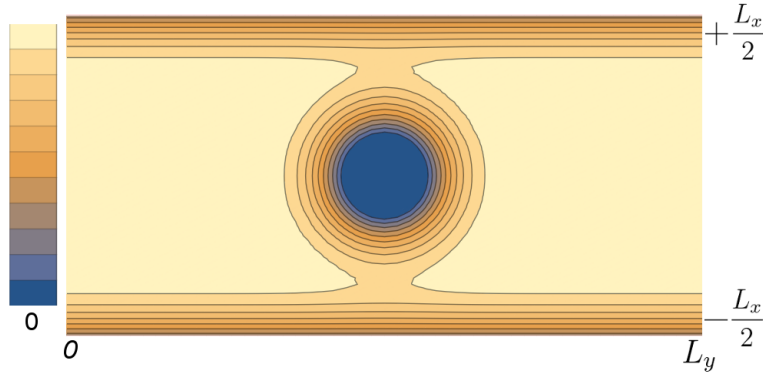


FIG. 9. $\rho_0(x, y, 0, \frac{L_y}{2})$, the ground state ($|+ + \dots +\rangle$) conditional probability density of finding a $C = +1$ electron somewhere given there is a $C = +1$ electron at position $(0, \frac{L_y}{2})$ on the cylinder. The correlation hole is isotropic. The (unrolled) cylinder periodicity in the y -direction is understood as matching $y = 0$ with $y = L_y$, and the number of available orbitals on the cylinder roughly lie in the segment between $(-\frac{L_x}{2}, \frac{L_x}{2})$, where $L_x = 2\pi N l_B^2 / L_y$. The system sizes here: $L_y = 15$, $l_B = 1$, and $N = 18$.

E. Understanding bilayer coherence: $H_{\frac{1}{2}\text{QH}}$ vs $H_{\mathbb{Z}_2}$

Here we present a simple picture for understanding the layer coherence of the bilayer QH problem. Consider electrons living on either of two parallel plates separated by a distance d , and label the two layers by a pseudospin $\alpha \in \{\uparrow, \downarrow\}$, where $\uparrow(\downarrow)$ is the upper(lower) layer. If the plates are infinite in extent and approximately uniform in charge with surface charge densities σ_α , then translational symmetry exists such that for the potential of either plate $\phi_\alpha(x, y, z) = \phi_\alpha(z)$. Such a problem is effectively a one-dimensional point charge with charge replaced by the charge density: $-\partial_z \phi_\alpha(z) = \sigma_\alpha \delta(z - z_\alpha)$ for a plates at $z_\uparrow = +d/2$ and $z_\downarrow = -d/2$, which has the solution $\phi_\alpha(z) = -\frac{1}{2}\sigma_\alpha |z - z_\alpha|$. The electric field between the two plates is uniform and parallel (or anti-parallel) to the uniform magnetic field $\mathbf{B} = \hat{z}B$. The electric charges q_\downarrow in the lower plate experience the field ϕ_\uparrow of the upper plate (and visa-versa), leading to our approximation for the inter-layer interaction:

$$\hat{V}_{\text{inter}} = \int d\mathbf{r} dz d\mathbf{r}' dz' c_\uparrow^\dagger(\mathbf{r}, z) c_\downarrow^\dagger(\mathbf{r}', z') \left(\frac{q_\downarrow \sigma_\uparrow |z - z'|}{-2} \right) c_\downarrow(\mathbf{r}', z') c_\uparrow(\mathbf{r}, z), \quad (28)$$

which, for electrons confined to their respective layers ($z = z_\uparrow$ and $z' = z_\downarrow$) reduces to:

$$= \int d\mathbf{r} d\mathbf{r}' c_\uparrow^\dagger(\mathbf{r}) c_\downarrow^\dagger(\mathbf{r}') \left(\frac{q_\downarrow \sigma_\uparrow d}{-2} \right) c_\downarrow(\mathbf{r}') c_\uparrow(\mathbf{r})$$

or even more simply (defining the constant $\lambda \equiv q_\downarrow \sigma_\uparrow / 2$ and the total number operators \hat{N}_α):

$$= -\lambda d \hat{N}_\uparrow \hat{N}_\downarrow.$$

Clearly, for a system with fixed particle number $\hat{N}_\alpha + \hat{N}_\beta = N$, the inter-layer interaction favours a state with $\hat{N}_+ = \hat{N}_- = N/2$. If we define pseudospin matrices $\tau_{\alpha\beta}^z$ to be the Pauli-Z $SU(2)$ generator, we can rewrite the inter-layer interaction as a out-of-plane coupling of electronic pseudospins plus a density-density piece

$$\hat{V}_{\text{inter}} = \int d\mathbf{r} d\mathbf{r}' \frac{-\lambda d}{2} c_\alpha^\dagger(\mathbf{r}) c_\beta(\mathbf{r}) \left(\mathbf{1}_{\alpha\beta} \mathbf{1}_{\alpha'\beta'} - \tau_{\alpha\beta}^z \tau_{\alpha'\beta'}^z \right) c_{\alpha'}^\dagger(\mathbf{r}') c_{\beta'}(\mathbf{r}'). \quad (29)$$

When written in this way, it is clear the second $\tau^z \otimes \tau^z$ term breaks $SU(2)$ symmetry, and additionally disfavors states with an imbalance between the total number of particles between the two layers. If we consider this inter-layer potential in addition to the layer-separation-independent interactions $H_{\frac{1}{2}\text{QH}}$, where we project all single-particle operators onto the LLL by substituting $c_\alpha(\mathbf{r}) \rightarrow \hat{c}_\alpha(\mathbf{r})$, we get the total Hamiltonian

$$H = H_{\frac{1}{2}\text{QH}} + \hat{V}_{\text{inter}}. \quad (30)$$

For $d = 0$, the two layers are not separated, and H reduces to $H_{\frac{1}{2}\text{QH}}$, which has a extensively degenerate ground state composed of polarized states and those connected to them by $SU(2)$ symmetry. Separating the layers ($d > 0$) by a small amount introduces anisotropy which splits the massively degenerate $SU(2)$ ground state manifold, driving up the polarized states in energy relative to those states with total $S_z = \int d\mathbf{r} c^\dagger(\mathbf{r}) \tau_z c(\mathbf{r}) = 0$.

For the scenario in which the two layers experience opposite sign magnetic fields ($H_{\mathbb{Z}_2}$), the ground state degeneracy is two-fold between fully polarized states, and there appears to exist a gap to the lowest excited states. Thus, no such instability exists.

F. 1D Ising transverse field as wall defect in 2D

Let us start with the one-body potential

$$\sum_{\mathbf{r}} c_+^\dagger(\mathbf{r}) f(\mathbf{r}) c_-(\mathbf{r}) \quad (31)$$

plus its hermitian conjugate. The one-body potential term $f(\mathbf{r})$ is a wall defect at $y = y_w$ along the length of the cylinder of circumference L_y :

$$f(\mathbf{r}) = \delta(y - y_w), \quad (32)$$

which has the orbital representation

$$= \sum_q e^{iq(y - y_w)}.$$

Because of the cylinders axial symmetry, the position of the wall y_w should be irrelevant. Projecting this onto the LLL (replacing $c_\pm(\mathbf{r}) \rightarrow \hat{c}_\pm(\mathbf{r})$ and plugging $f(\mathbf{r}) = \delta(y - y_w)$ into Eqn 31) follows as

$$\begin{aligned} & \sum_{\mathbf{r}} \hat{c}_+^\dagger(\mathbf{r}) f(\mathbf{r}) \hat{c}_-(\mathbf{r}) \\ &= \sum_{\mathbf{r}} \left(\sum_{k_y} e^{-ik_y y} e^{-\frac{1}{2l_B^2}(x - l_B^2 k_y)^2} d_{+,k_y}^\dagger \right) \delta(y - y_w) \left(\sum_{p_y} e^{ip_y y} e^{-\frac{1}{2l_B^2}(x + l_B^2 p_y)^2} d_{-,p_y} \right) \\ &= \sum_{k_y, p_y} d_{+,k_y}^\dagger d_{-,p_y} \sum_y \delta(y - y_w) e^{-i(k_y - p_y)y} \sum_x e^{-\frac{1}{2l_B^2}(x - l_B^2 k_y)^2} e^{-\frac{1}{2l_B^2}(x + l_B^2 p_y)^2}. \end{aligned}$$

Now using the Fourier transform of the delta-function $\delta(y - y_w) = \sum_q e^{iq(y-y_w)}$,

$$\begin{aligned}
&= \sum_{k_y, p_y} d_{+, k_y}^\dagger d_{-, p_y} \sum_y \left(\sum_q e^{iq(y-y_w)} \right) e^{-i(k_y - p_y)y} \sum_x e^{-\frac{1}{2l_B^2}(x - l_B^2 k_y)^2} e^{-\frac{1}{2l_B^2}(x + l_B^2 p_y)^2} \\
&= \sum_{k_y, p_y, q} d_{+, k_y}^\dagger d_{-, p_y} e^{-iqy_w} \sum_y e^{-i(k_y - p_y - q)y} \sum_x e^{-\frac{1}{2l_B^2}(x - l_B^2 k_y)^2} e^{-\frac{1}{2l_B^2}(x + l_B^2 p_y)^2} \\
&= \sum_{k_y, p_y, q} d_{+, k_y}^\dagger d_{-, p_y} e^{-iqy_w} \delta(p_y = k_y - q) \sum_x e^{-\frac{1}{2l_B^2}(x - l_B^2 k_y)^2} e^{-\frac{1}{2l_B^2}(x + l_B^2 p_y)^2} \\
&= \sum_{k_y, q} d_{+, k_y}^\dagger d_{-, k_y - q} e^{-iqy_w} \sum_x e^{-\frac{1}{2l_B^2}(x - l_B^2 k_y)^2} e^{-\frac{1}{2l_B^2}(x + l_B^2 (k_y - q))^2}.
\end{aligned}$$

Now note that the integral over x is a convolution of two Gaussians, one centered at $x = l_B^2 k_y$ and the other at $x = l_B^2 (k_y - q)$, with the largest contributions coming from those values of q such that the Gaussians overlap, i.e $q = 2k_y$. The non-dominant terms' contribution depends on the ratio of the magnetic length to the cylinder circumference l_B/L_y :

$$= \sum_{k_y} d_{+, k_y}^\dagger d_{-, -k_y} e^{i2k_y y_w} + \text{non-dominant}.$$

The peculiar phase factor is a consequence of the choice of $y = 0$. This can be gauged away by redefining the plane wave part of Eqn 5. Thus we get

$$\sum_{\mathbf{r}} c_+^\dagger(\mathbf{r}) f(\mathbf{r}) c_-(\mathbf{r}) + h.c = \sum_{k_y} d_{+, k_y}^\dagger d_{-, -k_y} + d_{-, -k_y}^\dagger d_{+, k_y} + \text{non-dominant}. \quad (33)$$

Keeping only the dominant terms, we see that the largest effect of the wall defect is to mix the Chern, similar to the Ising tranverse field mixing of the spin, where the local Pauli-X is defined

$$X_n = \frac{1}{2} \left(d_{+, n}^\dagger d_{-, -n} + d_{-, -n}^\dagger d_{+, n} \right). \quad (34)$$
